Int. J. Econ. Environ. Geol., Vol. 17, Issue 1, 2026, 60-69 doi: 10.46660/int.j.econ.environ.geol..v17i1.792
Journal home page: www.econ-environ-geol.org

GEOLOGY, MINERALOGY, AND ECONOMIC POTENTIAL OF A BANDED IRON FORMATION WITHIN THE PRECAMBRIAN BASEMENT OF THE MASIDPUR MAGNETIC BODY, NORTHWESTERN BANGLADESH

MD. SOHEL RANA*, MD. ALI AKBAR, MOHAMMED MASUM, MOHAMMED NURUL HOQUE, MD. NURUZZAMAN SABUJ AND MD ABU SAYEM
Geological Survey of Bangladesh, Segunbagicha, Dhaka-1000, Bangladesh

Received: *3 February, 2026* ***Accepted:*** *25 March, 2026*

Abstract: The Masidpur magnetic body, located at Alihat Union, Hakimpur Upazila, Dinajpur District, northwestern Bangladesh, contains geologically significant iron mineralization within the Precambrian crystalline basement of the Rangpur Saddle, a major basement high of the Bengal Basin. This study investigates the mineralogical composition, geochemical characteristics, iron mineralization, and geological significance of the deposit using integrated petrographic, mineralogical, and geochemical analyses. The investigation is based on four diamond drill holes completed by the Geological Survey of Bangladesh (GSB). A total of 98 basement core samples were examined using transmitted- and reflected-light petrography, X-ray fluorescence (XRF), X-ray diffraction (XRD), field-emission scanning electron microscopy coupled with energy-dispersive spectroscopy (FE-SEM/EDS), and inductively coupled plasma–optical emission spectrometry (ICP-OES). Petrographic analysis indicates that magnetite (average 27.75 wt.%) and quartz (average 44.47%) are the dominant mineral phases, accompanied by subordinate amphibole, pyroxene, mica, epidote, and feldspar. FE-SEM/EDS analyses corroborate the modal mineralogy, yielding average abundances of 26.84% iron minerals and 41.47% quartz. XRF analyses reveal average concentrations of 35.36 wt.% Fe_2O_3 and 39.50 wt.% SiO_2, whereas ICP-OES analyses of iron-rich intervals record Fe_2O_3 contents ranging from 46.20 to 77.67 wt.%. XRD patterns confirm magnetite–quartz as the principal crystalline assemblage with subordinate amphibole, mica, and feldspar. Iron-rich horizons occur consistently between depths of approximately 426 and 548 m, with an average cumulative thickness of ~50 m. Alternating magnetite-rich and silica-rich bands, together with their mineralogical, petrographic, and geochemical characteristics, indicate that the mineralization represents a metamorphosed banded iron formation (BIF) comparable to Precambrian BIFs worldwide. The integrated dataset establishes the Masidpur magnetic body as a geologically significant iron-mineralized system with promising exploration potential. However, its economic significance remains to be evaluated through additional drilling, resource estimation, metallurgical testing, and comprehensive feasibility studies.

Keywords: Magnetite, Precambrian basement, Banded Iron Formation (BIF), Iron ore mineralization.

Introduction

The first iron ore deposit in Bangladesh was discovered at Alihat Union of Hakimpur Upazila, Dinajpur District in the northwestern part of the country (Fig. 1). The study area is bounded by Nawabganj Upazila to the north, Birampur to the northwest, Panchbibi to the south, and Ghoraghat to the east, covering an area of approximately 5 km². Geologically, this region forms part of the Rangpur Saddle, a prominent Precambrian crystalline basement high in northern Bangladesh that has long been considered prospective for iron ore and associated economic mineralization (Ahmed *et al*., 2015). The area is represented on the Survey of Bangladesh topographic sheet No. 78C/15 at a scale of 1:50,000.

Systematic exploration of the region began in 2000, when the Geological Survey of Bangladesh (GSB) conducted a regional geophysical investigation, including magnetic surveys, across northwestern Bangladesh. These surveys identified two prominent zones of high magnetic susceptibility in the Hakimpur and Kutubpur areas of Dinajpur District (Fig. 2a), suggesting the presence of magnetite-rich basement lithologies. Subsequently, under the Geoscience Project, GSB carried out a detailed high-resolution magnetic survey in 2012, which delineated a discrete, high-intensity magnetic body with an aerial extent of approximately 5 km² in the Masidpur–Alihat area (Fig. 2b).

To verify the subsurface source of the magnetic anomaly, GSB initiated a diamond drilling program in 2013, drilling borehole GDH-68/13 at Chakupara–Masidpur in Hakimpur Upazila (Fig. 3). This borehole intersected three high-grade iron ore horizons at depths of approximately 458 m, 573 m, and 584 m, respectively confirming the

*Corresponding author e-mail: sohelgsb@gmail.com

presence of significant iron mineralization. In order to further evaluate the geometry, continuity, and grade variation of the deposit, three additional boreholes, GDH-73/19, GDH-74/19, and GDH-75/20 were subsequently drilled as part of the continuing exploration program. These boreholes revealed multiple iron ore–bearing horizons, with an average cumulative thickness of approximately 50m (Masum *et al*., 2021), indicating a laterally persistent and geologically significant iron ore system.

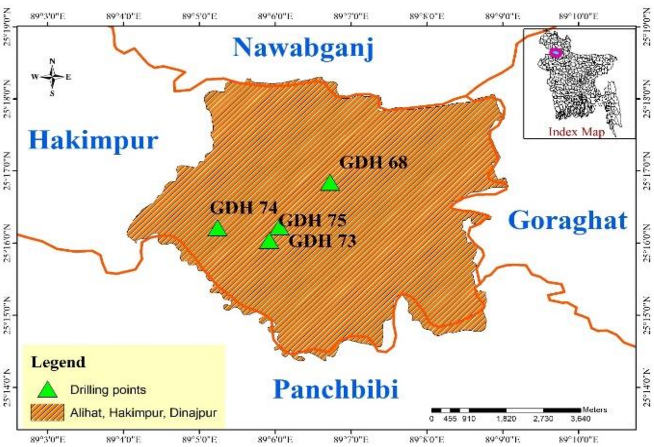

Fig. 1 Location map of study area at Alihat Union of Hakimpur upazila, Dinajpur, Bangladesh.

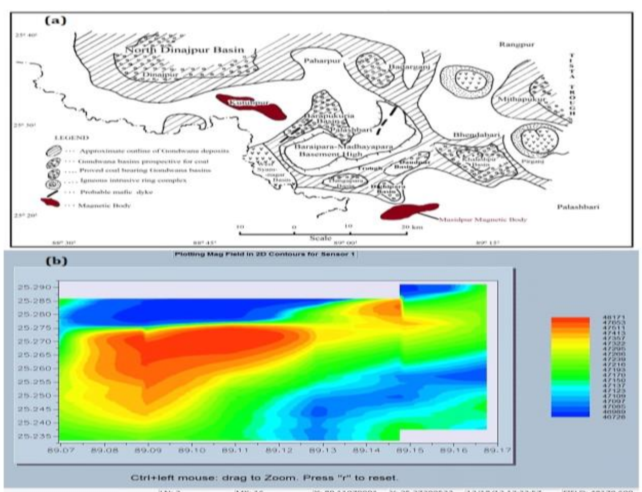

Fig. 2 a) high magnetic signatures b) high magnetic susceptibility map of Masidpur magnetic body at Alihat Union of Hakimpur upazila, Dinajpur, Bangladesh. (modified from Rahman et.al. 2000).

Development of the Masidpur deposit faces technical, economic, and environmental challenges: limited drilling constrains resource continuity depths exceeding 400 m increase mining costs magnetite–silicate interbanding complicates beneficiation; and groundwater management, waste disposal, and land-use impacts require careful mitigation. Addressing these issues will require integrated geological, metallurgical, and environmental studies prior to commercial development (Klein, 2005; Rollinson, 2014). Despite detailed characterization, key gaps remain: limited drilling precludes a compliant resource estimate additional drilling and 3D modelling are required beneficiation parameters and impurity behaviour are unresolved and depositional age and tectono-metamorphic evolution require isotopic and trace-element studies. Future research should integrate geophysical modelling, metallurgical testing, and economic feasibility analysis to support sustainable resource development (Gross, 1980; Klein, 2005; Rollinson, 2014).

Geological Setting

The investigated area is located within the Rangpur Platform, a tectonic province characterized by shallowly buried Precambrian basement rocks. Structurally, the study area forms part of the Dinajpur Slope of the Rangpur Saddle, a prominent basement high in northwestern Bangladesh. The Rangpur Platform is widely interpreted as the subsurface continuation of the Indian Shield, extending between the Rajmahal Hills to the west and the Shillong Massif to the east (Rahman *et al*., 1990). The Rangpur Saddle is structurally complex and is marked by alternating horst and graben systems, which are clearly reflected in regional gravity anomaly maps as gravity highs and lows, indicating differential basement uplift and subsidence (Fig. 3).

The depth to the crystalline basement within the Rangpur Platform varies significantly, ranging from approximately 128 m to about 1.0 km. The shallowest basement occurrence recorded to date is at a depth of 128 m in the Madhyapara area, Dinajpur District. Gondwana sedimentary sequences are preserved only within fault-bounded basins developed within the basement complex, suggesting syn-tectonic deposition during post-basement extensional events. In some areas, Tertiary sedimentary rocks directly overlie the Precambrian basement or rest unconformably above the Gondwana succession. The Tertiary stratigraphy of the Rangpur Saddle area is dominated by the Tura Formation and the overlying Dupi Tila Formation. These units are, in turn, overlain by Pleistocene Madhupur Clay and Recent alluvial deposits. In the southern slope of the adjacent Bogra Shelf, additional sedimentary units such as the Surma Group, Kopili Formation, and Sylhet Limestone have been reported (Zaher *et al*., 1980).

Within the Masidpur magnetic body, iron-bearing layers occur at the top of the Precambrian basement complex. The iron ore is typically black to brownish-black in color, exhibits a metallic luster, high magnetic susceptibility, and high specific gravity, and produces a characteristic black streak features consistent with magnetite-rich mineralization. With increasing depth, the basement lithology is dominated by alternating gneiss and quartzite units. The gneisses are generally light gray to medium gray in color, although greenish-gray varieties have been observed in borehole GDH-75/20. Quartzites are predominantly white to pink, hard, and crystalline in nature. The lithological association and stratigraphic position of the iron-bearing horizons suggest a basement-hosted iron formation genetically linked to Precambrian tectono-metamorphic processes.

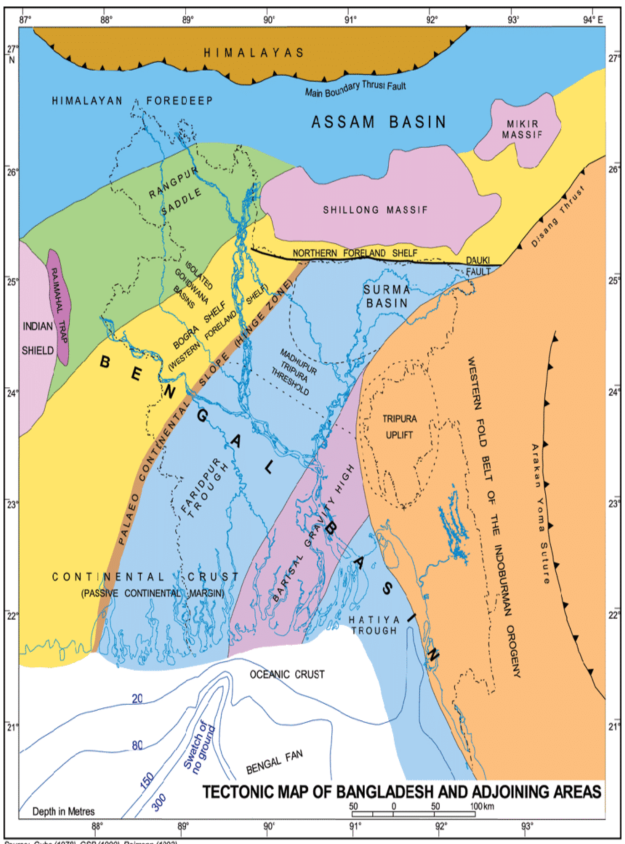

Fig. 3 Regional geological and tectonic setting of the Bengal Basin (Guha, 1978; GSB, 1990; Reimann, 1993).

Materials and Methods

A total of 98 basement core samples were collected from four diamond drill holes (GDH-68/2013, GDH-73/2019, GDH-74/2019, and GDH-75/2020) intersecting the mineralized interval of the Masidpur magnetic body. Samples were systematically selected from representative lithological units, magnetite-rich horizons, and silica-rich bands to capture the deposit's mineralogical and geochemical variability. Petrographic study was carried out on 30 representative samples using standard and polished thin sections. Mineral identification, modal composition, alteration, and textural relationships were examined under transmitted-light (TL) and reflected-light (RL) polarized microscopy. Quantitative modal analyses employed approximately 300 point counts per thin section, providing statistically reliable mineral abundance estimates (Chayes, 1956; Deer *et al*., 2013; Nesse, 2017).

Representative subsets were analyzed by X-ray fluorescence (XRF) for major-element determination, X-ray diffraction (XRD) for mineral phase identification, field-emission scanning electron microscopy coupled with energy-dispersive spectroscopy (FE-SEM/EDS) for mineral chemistry and micro-textural characterization, and inductively coupled plasma–optical emission spectrometry (ICP-OES) for selected major and trace element analyses (Potts, 1987; Reed, 2005; Rollinson, 2014). Quality assurance included standardized core logging, documented chain-of-custody procedures, instrument calibration, certified reference materials (CRMs), procedural blanks, duplicate analyses where applicable, and routine internal quality-control checks. These QA/QC measures ensured analytical accuracy, precision, reproducibility, and the generation of robust datasets suitable for mineralogical, petrographic, and geochemical interpretation (Thompson and Howarth, 1978; Potts, 1987).

Sample Collection

Exploratory drilling in the Masidpur area was conducted by the Geological Survey of Bangladesh using standard mineral exploration techniques, employing an LF Core Drill–90 rig (Fig.4a) with drilling mud circulation for optimal core recovery and borehole stability. Four diamond drill holes were completed, and high-quality basement core samples (Fig. 4b) were recovered via wireline drilling, then systematically logged and preliminarily examined using hand lens, color, and grain-size charts.

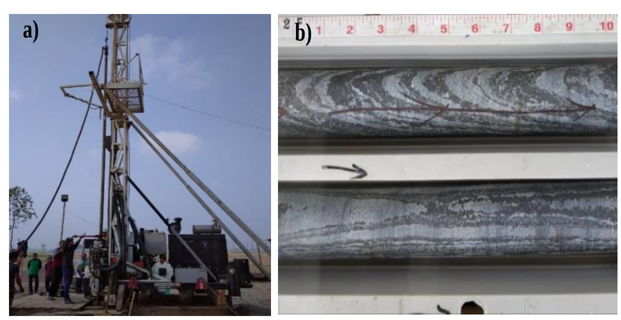

Fig. 4 Photographs showing (a) the LF Core Drill–90 drilling rig and (b) representative basement rock core samples.

Lithological characteristics—including color, texture, grain size, mineral content, degree of alteration, and structural features — were carefully recorded in field log sheets and notebooks following established geological logging procedures (Moon *et al*., 2006; Marjoribanks, 2010). These field observations formed the basis for subsequent laboratory-based mineralogical and geochemical analyses.

Microscopic Methods

Petrographic analysis was performed using a ZEISS Axio Scope.A1 polarizing microscope in transmitted- and reflected-light modes at the Geological Survey of Bangladesh. Polished thin sections were prepared, and minerals identified by optical properties, while opaque phases, especially iron oxides, were examined for reflectance, anisotropy, and texture. Quantitative modal mineral abundance was estimated using the standard point-counting technique on thin sections, providing statistically representative mineral proportions and supporting petrographic interpretations (Deer *et al*., 2013; Hutchison, 1974). The combined use of transmitted- and reflected-light microscopy ensured reliable identification of both silicate and ore mineral phases relevant to iron ore characterization.

Field Emission Scanning Electron Microscope (FE-SEM) Methods

Field Emission Scanning Electron Microscopy (FE-SEM) was used to investigate micro-textures and mineral chemistry of iron-bearing phases from the Masidpur magnetic body. High-resolution imaging using a GEMINI-based system enabled detailed observation of grain boundaries and mineral associations. Secondary and backscattered electron imaging distinguished topography and compositional contrasts. Elemental analyses were performed using EDS for qualitative to semi-quantitative data and WDS for higher-resolution measurements.

This integrated approach allowed precise characterization of magnetite, associated silicates, and trace elements, including thorium and rare earth elements. EDS-based quantitative elemental analyses were applied to representative samples from the Masidpur magnetic body to support petrographic observations and bulk geochemical data. The integration of high-resolution imaging and micro-analytical techniques provided critical insights into mineral associations, textural controls, and compositional variability of the iron ore system (Goldstein *et al*., 2018; Reed, 2005).

X-ray Fluorescence (XRF) Spectroscopy Methods

Major and minor element compositions of representative samples from the Masidpur magnetic body were determined using X-ray Fluorescence (XRF) spectroscopy at the IMMM Laboratory. Analyses were carried out using a Rigaku ZSX Primus wavelength-dispersive XRF spectrometer equipped with a 4 kW Rh-anode end-window X-ray tube, following established analytical procedures described by Goto and Tatsumi (1994, 1996). Major and trace elements were analyzed under optimized XRF conditions heavy elements at 40 kV and 60 mA, and light elements at 30 kV and 100 mA. Accuracy was ensured using GSJ reference materials (JSD-1, JSD-2, JSD-3). Element-specific crystals (LiF1, Ge, PET, RX25) improved precision. Analytical uncertainties were within ±1% for major elements and ±5% for trace elements, reported as oxide wt.%.

X-ray Diffraction (XRD) Methods

Bulk rock samples from four drill holes were prepared for XRD following standard protocols. Samples were micronized in ethanol, dried at 60 °C, homogenized, and mounted to minimize preferred orientation. Data were collected using a Rigaku Ultima IV diffractometer with a cobalt X-ray source at 40 kV and 40 mA. Samples were rotated during scanning over 5°–140° 2θ. Diffraction patterns were recorded using a PIXcel 1D detector. Phase identification was performed with Rigaku software (v4.5) using the ICDD PDF-2 database. Quantitative phase analysis (QPA) was carried out using Rietveld refinement techniques implemented in the Integrated X-ray Powder Diffraction Software (PDXL, Rigaku, Japan), enabling determination of relative mineral abundance and confirmation of dominant and subordinate crystalline phases (Young, 1993; Bish and Post, 1993).

Inductively Coupled Plasma–Optical Emission Spectrometry (ICP-OES) Method

Twenty representative samples from iron-rich zones of the Masidpur magnetic body were analyzed using ICP-OES (Varian 710-ES) to quantify major and trace elements. Samples were nebulized into an argon plasma generated by a high-frequency induction coil, achieving temperatures of 6,000–10,000 K for efficient atomization and excitation. Emitted element-specific radiation was measured spectrometrically, and concentrations were determined using calibration curves based on certified reference standards, ensuring accurate multi-element geochemical analysis. This technique provides high analytical precision, low detection limits, and reliable quantification of iron and associated elements in ore-bearing samples (Boss and Fredeen, 2004; Rollinson, 2014).

Results and Discussion

Microscopic Analysis

Quantitative modal analysis of thirty representative basement samples from four drill holes (GDH-68/13, GDH-73/19, GDH-74/19, and GDH-75/20) identified seven principal mineral phases: magnetite, quartz, amphibole, pyroxene, mica, epidote, and feldspar (Table 1, Fig. 5). Modal abundance was determined using the point-counting method, providing statistically reliable mineral proportions and ensuring consistency among samples (Chayes, 1956; Deer *et al*., 2013).

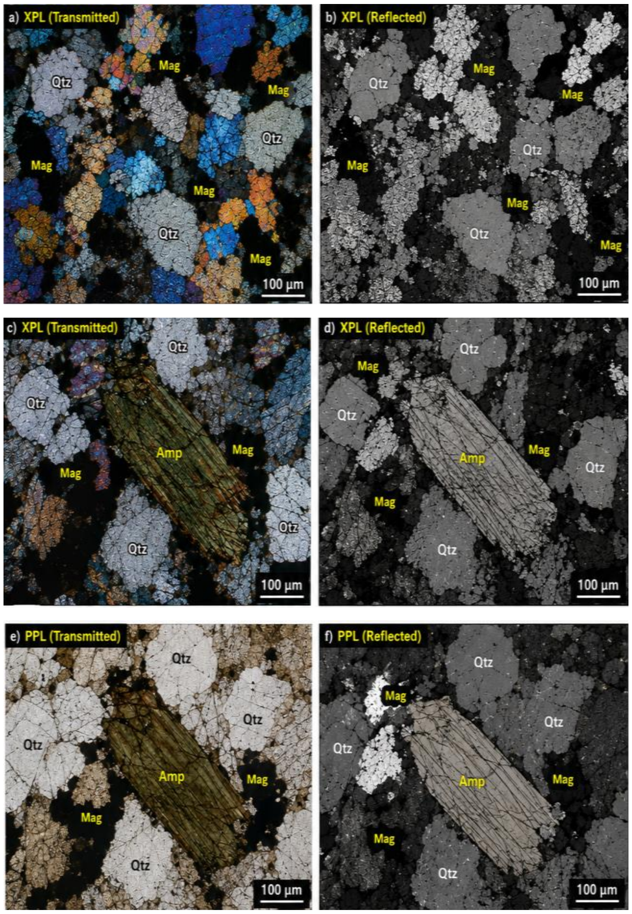

Fig. 5 Representative photomicrographs illustrating the mineralogical characteristics of selected basement core samples. Sample GDH-73/19/S-4 shows (a) transmitted light under crossed polars (XPL, 10×) and (b) reflected light under crossed polars (XPL, 10×). Sample GDH-74/19/S-3 displays (c) transmitted light under crossed polars (XPL, 10×) and (d) reflected light under crossed polars (XPL, 10×). Sample GDH-75/20/S-1 presents (e) transmitted light under plane-polarized light (PPL, 10×) and (f) reflected light under plane-polarized light (PPL, 10×). The photomicrographs reveal the presence of quartz (Qtz), magnetite (Mag), and amphibole (Amp).

Magnetite is the dominant ore mineral, ranging from 6.5 to 57.3 wt% (average 27.75 wt%). Under reflected light, magnetite appears bright creamy-white, isotropic, highly reflective, and commonly occurs as coarse anhedral to subhedral grains, disseminations, and discontinuous bands. Locally, grains display interlocking contacts with quartz and minor microfractures, indicating recrystallization during metamorphism. Quartz, the principal gangue mineral, ranges from 26.8 to 62.1 wt% (average 44.47 wt%) and is recognized in transmitted light by its low relief, absence of cleavage, low first-order grey interference colours, and undulose extinction, reflecting deformation and dynamic recrystallization.

Amphibole (average 8.01 wt%) occurs as elongated to prismatic crystals exhibiting moderate-to-high relief, two cleavage directions intersecting at approximately 56° and 124°, and characteristic green to brown pleochroism. Pyroxene (average 1.72 wt.%) is distinguished by higher relief, nearly 90° cleavage, weak pleochroism, and first- to second-order interference colours. Mica (average 8.83%) occurs mainly as biotite, showing perfect basal cleavage, strong pleochroism, and bird's-eye extinction, whereas epidote (average 1.37 wt.%) exhibits high relief, pistachio-green colour, and high-order interference colours. Feldspar (average 2.93 wt%) is identified by low relief, polysynthetic twinning in plagioclase, and locally sericitized grains. These optical observations are consistent with the XRD results, which confirm magnetite, quartz, amphibole, feldspar, mica, pyroxene, and epidote as the principal crystalline phases.

FE-SEM/EDS analyses further verify mineral identification through characteristic elemental compositions, including Fe-rich magnetite, Si-rich quartz, Fe–Mg-bearing amphibole and pyroxene, K-rich mica, Ca–Al-rich epidote, and Na–Ca-bearing feldsparThe combined petrographic, XRD, and FE-SEM/EDS evidence demonstrates that the Masidpur magnetic body comprises magnetite-rich quartzofeldspathic rocks with subordinate ferromagnesian silicates, consistent with a metamorphosed Precambrian banded iron formation (Gross, 1980; Klein, 2005; Deer *et al*., 2013).

X-ray Fluorescence (XRF) Spectroscopy Analysis

Total 26 (Twenty six) basement samples have been analyzed for X-ray Fluorescence (XRF) Spectroscopy analysis of the Masidpur magnetic body in Institute of Mining, Mineralogy and Metallurgy (IMMM), BCSIR, laboratory of Joypurhat. The XRF results (Table 2) provide a comprehensive overview of the major and minor oxide geochemistry of the iron-bearing basement sequence.

The analyzed samples are dominated by Fe_2O_3 and SiO_2, reflecting the prevalence of magnetite and quartz observed in petrographic investigations. Fe_2O_3 contents vary widely, ranging from moderate concentrations (~25–30 wt. %) to very high values exceeding 70 wt.% in several samples, particularly from drill hole GDH-73/19. These elevated Fe_2O_3 concentrations define high-grade iron-rich horizons within the basement complex. In contrast, SiO_2 contents range from approximately 23 to >65 wt. %, corresponding to silica-rich layers and quartz-dominated bands. The pronounced inverse relationship between Fe_2O_3 and SiO_2 is a characteristic geochemical feature of banded iron formation (BIF)–type deposits. Al_2O_3, MgO, and CaO occur in variable but generally subordinate proportions, consistent with the presence of amphibole, pyroxene, mica,

Table 1. Mineralogical composition of Masidpur magnetic body at Alihat in Dinajpur.

Sample No	Depth	Magnetite	Quartz	Amphibole	Pyroxene	Mica	Epidote	Feldspar	Others
GDH-68/13.S-1	450 m	08.80	56.20	09.20	01.60	09.60	00.40	07.80	06.40
GDH-68/13.S-2	460 m	14.10	47.10	10.80	01.30	10.90	01.30	08.20	06.30
GDH-68/13.S-3	487 m	08.30	55.00	07.10	02.90	10.40	01.30	09.70	05.30
GDH-68/13.S-4	514 m	21.80	40.90	09.00	01.40	06.60	00.40	15.40	04.50
GDH-68/13.S-5	524 m	06.50	62.00	08.90	02.30	06.70	00.30	07.70	05.60
GDH-68/13.S-6	530 m	13.60	49.60	12.90	02.40	07.20	01.20	08.10	05.00
GDH-68/13.S-7	540 m	12.60	50.50	13.00	02.00	07.30	03.10	06.00	05.50
GDH-68/13.S-8	545 m	06.70	57.20	14.20	02.70	05.40	02.70	05.30	05.80
GDH-73/19.S-1	429 m	36.50	46.10	06.60	01.40	03.90	01.10	00.00	04.40
GDH-73/19.S-2	432 m	50.30	40.80	02.10	00.70	01.30	00.20	00.40	04.20
GDH-73/19.S-3	537 m	55.60	28.00	04.80	01.40	03.70	00.70	00.30	05.50
GDH-73/19.S-4	439 m	47.90	35.00	05.70	01.50	02.70	01.70	00.00	05.50
GDH-73/19.S-5	441 m	49.70	35.60	02.90	01.20	02.50	00.90	02.00	05.20
GDH-73/19.S-6	449 m	51.00	27.10	06.50	01.90	04.90	02.00	00.30	06.30
GDH-73/19.S-7	454 m	57.30	30.60	01.80	01.00	03.10	00.60	00.00	05.60
GDH-73/19.S-8	457 m	55.20	26.80	04.30	02.70	04.40	01.00	00.20	05.40
GDH-74/19.S-1	435 m	31.00	46.20	02.70	01.40	14.20	01.20	00.00	03.30
GDH-74/19.S-2	449 m	23.60	49.10	09.70	01.50	09.00	01.10	01.20	04.80
GDH-74/19.S-3	458 m	25.70	47.90	09.60	01.00	09.50	01.20	00.70	04.40
GDH-74/19.S-4	465 m	22.70	52.70	05.50	01.60	09.80	01.50	01.20	05.00
GDH-74/19.S-5	481 m	14.50	61.10	05.00	01.50	09.40	01.40	02.30	04.80
GDH-74/19.S-6	491 m	14.30	62.10	05.50	02.20	09.40	01.10	01.50	03.90
GDH-74/19.S-7	534 m	13.40	49.80	13.30	02.00	13.10	01.40	02.30	04.70
GDH-75/20.S-1	427 m	31.30	31.90	14.50	01.50	09.70	02.60	02.70	05.80
GDH-75/20.S-2	429 m	29.20	35.50	14.10	02.50	11.90	01.60	00.40	04.80
GDH-75/20.S-3	437 m	24.50	41.80	08.70	02.90	16.10	03.10	00.00	02.90
GDH-75/20.S-4	442 m	28.20	38.60	10.50	02.20	10.60	02.10	03.40	04.40
GDH-75/20.S-5	444 m	29.70	38.10	05.70	01.90	16.10	03.60	00.80	04.10
GDH-75/20.S-6	448 m	24.70	40.30	10.20	00.30	20.50	00.20	00.00	03.80
GDH-75/20.S-7	453 m	23.80	50.50	05.60	00.80	15.10	00.10	00.00	04.10
Average		**27.75**	**44.47**	**08.01**	**01.72**	**08.83**	**01.37**	**02.93**	**04.91**

Table 2. X-ray Fluorescence (XRF) spectroscopy analysis of the Masidpur magnetic body at Alihat in Dinajpur.

Sample no	Depth(m)	Na_2O	MgO	Al_2O_3	SiO_2	P_2O_5	SO_3	Cl	K_2O	CaO	TiO_2	V_2O_5	Cr_2O_3	MnO	Fe_2O_3	Co_2O_3	NiO	CuO	ZnO	Ga_2O_3	Rb_2O	SrO	Y_2O_3	ZrO_2
GDH-68/13.S-1	412	0.16	1.18	3.35	7.53	0.08	0.4	0	0.43	83.2	0.23	-	0.05	0.42	2.85	0.007	-	-	-	-	0.003	0.07	-	-
GDH-68/13.S-2	440	0.09	1.33	3.88	15.6	0.06	0.6	0	0.82	71.8	0.33	-	0.11	0.49	4.76	-	0	-	0	-	0.003	0.07	-	0.016
GDH-68/13.S-3	481	2.74	2.57	16.29	60.6	0.17	0.1	0.1	4.84	5.15	0.47	-	0.28	0.09	6.36	-	0	0.01	0	-	0.011	0.07	-	-
GDH-68/13.S-4	460	3.06	4.5	16.92	51.2	0.29	0.1	0.2	2.66	8.34	0.92	-	0.22	0.21	11.15	-	0	0.01	0	0.005	0.008	0.06	0.01	0.008
GDH-68/13.S-5	421	2.23	4	14.03	61.8	0.05	0.2	0.1	3.3	3.95	0.92	-	0.44	0.09	8.48	-	0	0.02	0	-	0.013	0.04	-	0.034
GDH-68/13.S-6	520	2.85	6.8	20.52	41.7	0.34	0	0.2	6.1	6.07	1.71	-	0.1	0.15	12.84	0.005	0	-	0	0.005	0.026	0.09	-	0.062
GDH-68/13.S-7	478	2.19	4.96	16.16	44.8	0.33	0.1	0.1	1.61	14.4	1.03	0.05	0.18	0.24	13.54	-	0	0.01	0	-	0.004	0.08	-	0.006
GDH-68/13.S-8	540	1.56	10.2	13.78	41.8	0.7	0.2	0.1	3.55	10.2	1.86	-	0.17	0.27	15.06	-	0	0.01	0	-	0.012	0.08	0	0.027
GDH-68/13.S-9	535	3.32	1.32	16.66	65.3	0.11	0.1	0	2.93	5.04	0.37	0.01	0.35	0.06	4.079	-	0	0.01	0	-	0.007	0.1	-	0.016
GDH-68/13.S-10	542	1.72	7.69	14.81	45.7	0.23	0.2	0.1	2.51	10.4	1.17	-	0.29	0.27	14.72	-	0	0.01	0	-	0.01	0.06	-	0.01
GDH-68/13.S-11	610	3.84	1.76	15.63	61.2	0.13	0.7	0	1.3	4.66	0.68	-	0.32	0.08	9.43	0	0	0.05	0	-	0	0.08	-	0.01
GDH-68/13.S-12	573	2.66	1.02	9.96	35	0.06	0.1	0	0.48	2.78	2.24	-	0.24	0.27	45.06	-	0		0.1	-	-	0.02	-	0.01
GDH-73/19.S-1	432	0.08	0.42	1.21	43.6	0.26	0	0	0.05	1.07	-	-	0.64	0.18	52.42	-	-	-	-	-	-	-	-	0.01
GDH-73/19.S-2	433	0.02	0.34	0.46	40.9	1.27	0	0	0.01	2.11	-	-	0.75	0.1	53.96	-	0	-	-	-	-	-	-	0.01
GDH-73/19.S-3	434	0.04	0.5	0.67	47.7	0.4	0	0	0.11	0.54	0.03	-	0.34	0.4	48.57	-	-	-	-	0.02	-	-	0.01	-
GDH-73/19.S-4	436	0.05	0.6	0.96	38.1	1.16	0	0	0.18	2.85	0.04	-	0.51	0.15	55.23	0.01	-	-	-	0.05	0.01	-	0.01	0.05
GDH-73/19.S-5	437	0.04	0.25	0.41	30.2	1.05	0	0.1	0.01	1.62	-	-	0.035	0.11	65.65	-	-	-	-	-	-	-	-	0.01
GDH-73/19.S-6	439	0.02	0.75	0.81	30.8	0.48	0	0	0.02	5.41	0.02	-	0.55	0.22	60.89	0.01	-	-	-	0.03	-	-	0.01	-
GDH-73/19.S-7	441	0.03	0.42	0.4	22.9	0.22	0	0	0.01	0.69	-	-	0.34	0.22	74.68	-	-	-	-	-	-	-	-	0.01
GDH-73/19.S-8	442	0.13	1.86	1.13	32.9	3.32	0	0.1	0.16	5.79	0.04		0.74	0.14	53.56	0.01	0	-	-	-	-	0.01	0.01	0.01
GDH-73/19.S-9	444	0.29	1.81	2.25	40.4	0.4	0	0	0.21	1.74	0.15		0.57	0.24	51.94		0		0			0.01		0.01
GDH-73/19.S-10	447	0.05	1.26	0.99	33.6	1.07	0	0	0.03	3.13	0.05	-	0.45	0.13	59.12	0.01	-	-	-	0.04	-	-	0.01	-
GDH-73/19.S-11	449	1.79	3.95	10.37	47.7	0.73	0	0	0.79	6.98	0.53	0.02	0.55	0.19	26.07	0.02	-	0.01	-	0.02	0.07	0	0.01	0.12
GDH-73/19.S-12	454	0.03	0.74	0.75	35.6	1.05	0	0	0.01	6.75	-	-	0.1	0.19	54.33	-	-	-	-	-	-	0.01	-	0.01
GDH-73/19.S-13	457	0.09	2.03	1.27	26.3	3.97	0	0.1	0.06	9.05	0.06	-	0.6	0.19	56.07	-	0	-	0	-	-	0.01	0.01	0.01
GDH-73/19.S-14	428	0.67	3.39	5.88	24.9	0.96	0	0	0.59	3.64	0.2	0	0.44	0.43	58.76	-	0	-	0	-	-	0.01	-	0.01

epidote, and feldspar as accessory silicate minerals. TiO_2 concentrations are uniformly low (<2 wt. %), suggesting limited contribution from Ti-bearing oxide phases such as ilmenite. P_2O_5 contents are also generally low (<1 wt. %), indicating minor apatite, monazite, allanite involvement and limited phosphorus enrichment. Trace oxides, including MnO, V_2O_5, and Cr_2O_3, occur in low concentrations but are locally enriched within magnetite-rich layers, reflecting their affinity for iron oxide phases during deposition and metamorphism.

Overall, the XRF geochemical signatures demonstrate strong stratigraphic and compositional banding between iron-rich and silica-rich layers, consistent with Precambrian BIF systems worldwide. When integrated with mineralogical and microscopic data, these resultsconfirm that the Masidpur magnetic body hosts a magnetite-dominated iron formation with significant economic potential and warrants further resource evaluation (Gross, 1980; Klein, 2005; Rollinson, 2014).

X-Ray Diffraction (XRD) Analysis

Total 10 (Ten) basement samples have been analyzed for XRD analysis in Bangladesh Petroleum exploration and production Company Limited (BAPEX) laboratory of the Petrobangla. X-ray diffraction (XRD) analyses of representative basement rock smples from the Masidpur magnetic body confirm the dominance of magnetite and quartz as the principal mineral phases, consistent with petrographic and geochemical observations. The two XRD patterns display strong, well-defined diffraction peaks corresponding to magnetite (Fe_3O_4) and quartz (SiO_2), indicating that these minerals constitute the major crystalline components of the iron-bearing sequence. The high intensity of magnetite reflections in one of the diffractograms reflects iron-rich horizons, whereas the relative enhancement of quartz peaks in the second pattern corresponds to silica-dominant bands within the stratigraphy.

Subordinate diffraction peaks attributable to amphibole, mica, feldspar, and minor pyroxene are also observed, indicating the presence of accessory silicate phases associated with metamorphosed iron formations (Fig. 6). The absence or very low intensity of peaks related to hematite suggests that iron mineralization is predominantly magnetite-bearing rather than oxidized iron ore. Additionally, the sharpness and symmetry of major peaks imply a moderate to high degree of crystallinity, likely resulting from regional metamorphic recrystallization of the original chemical sediments.

The alternation of magnetite-rich and quartz-rich assemblages identified in the XRD patterns is characteristic of banded iron formation (BIF)–type deposits. Such mineralogical associations are widely reported from Precambrian iron formations worldwide and reflect primary chemical banding subsequently modified by metamorphism (Gross, 1980; Klein, 2005). The XRD results therefore provide robust mineralogical confirmation that the Masidpur magnetic body represents a magnetite-dominated Precambrian iron formation with significant geological and economic relevance.

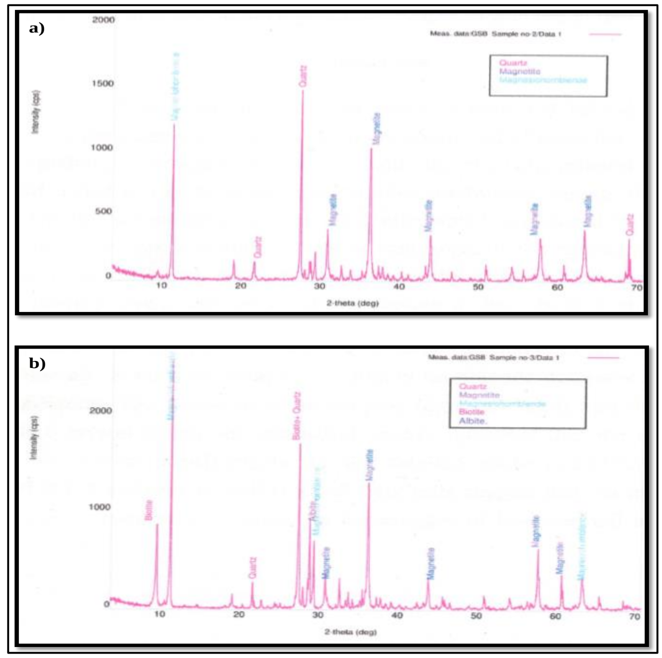

Fig. 6 Qualitative X-ray diffraction (XRD) patterns of representative samples from the study area: (a) sample GDH-74/19/S-2 and (b) sample GDH-75/20/S-3, illustrating the identified mineral phases.

FE-SEM Analysis

A total of twelve (12) representative basement samples collected from four drill holes of the Masidpur magnetic body were investigated using Field Emission Scanning Electron Microscopy (FE-SEM) coupled with Energy Dispersive X-ray Spectroscopy (EDS). In total, 196 EDS spot analyses were performed to obtain quantitative elemental compositions of individual mineral phases and to verify mineralogical interpretations derived from petrographic and XRD analyses (Fig. 7).

The FE-SEM–EDS results indicate that the basement assemblage is mineralogically heterogeneous but dominated by iron-bearing and siliceous phases. Seven (7) major mineral groups were identified across the analyzed samples (Table 3), including magnetite, quartz, feldspar, amphibole, pyroxene, mica, and epidote. Magnetite is the principal ore mineral, with modal proportions ranging from 5.88 to 47.05%, and an average abundance of 26.84%, confirming significant iron enrichment within the basement sequence. Quartz constitutes the main gangue phase, varying from 29.41 to 64.70% with an average of 41.47%.

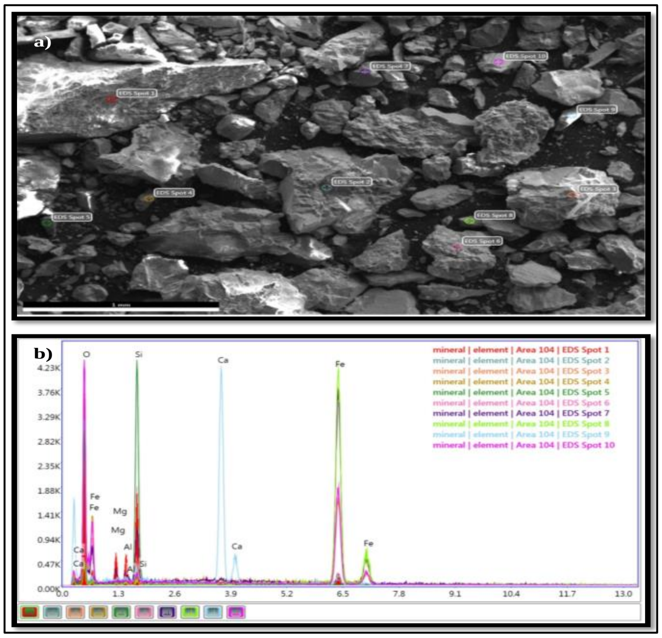

Fig. 7 FE-SEM–EDS results for sample GDH-74/2019/S-1: (a) energy-dispersive X-ray spectroscopy (EDS) spectrum obtained from spot analysis, and (b) EDS elemental phase analysis illustrating the distribution of major constituent elements.

Silicate minerals occur in subordinate but variable amounts, including amphibole (0.00–23.52%; average 8.19%), feldspar (0.00–23.52%; average 7.42%), mica (0.00–11.76%; average 3.01%), pyroxene (0.00–5.90%; average 1.96%), and epidote (0.00–5.88%; average 0.49%). Minor and unidentified phases collectively comprise 5.88–17.67% corroborate optical microscopy and XRD findings, provide robust confirmation of a magnetite-dominated iron formation with economic significance (Gross, 1980; Klein, 2005; Goldstein *et al*., 2018).

ICP-OES Analysis

ICP-OES analyses of twenty iron ore–bearing core samples from the Masidpur magnetic body were conducted using a Varian 710-ES at GSB to quantify iron in high-grade zones. Ten samples each from GDH-73/19 and GDH-75/20 represent mineralized intervals at varying depths. Results show consistently high Fe_2O_3 contents ranging from 46.20 to 77.67 wt.%, (Table 4) with most samples between ~59 and 78 wt.% and several exceeding 70 wt.%. These values indicate medium- to high-grade magnetite-dominated mineralization, comparable to economically viable Precambrian BIF deposits worldwide.

The observed variability in Fe_2O_3 content reflects stratigraphic banding and heterogeneous distribution of magnetite-rich layers interbedded with silica-rich bands, as confirmed by petrographic, XRD, and XRF analyses. The strong agreement between bulk geochemical data and mineralogical observations supports the interpretation of the Masidpur magnetic body as a magnetite-dominated BIF system. From a metallogenic perspective, the high Fe_2O_3 values highlight the significant economic potential of the deposit and justify further resource estimation and beneficiation studies (Gross, 1980; Klein, 2005; Rollinson, 2014).

Table 3. Average mineral percentage of the Masidpur magnetic body in Dinajpur wt.%.

Sample No	Depth	Magnetite	Quartz	Amphibole	Pyroxene	Mica	Epidote	Feldspar	Others
GDH-68/13.S-1	421 m	05.88	29.41	23.52	00.00	00.00	00.00	23.52	17.67
GDH-68/13.S-4	514 m	23.52	35.29	11.76	05.88	00.00	00.00	11.76	11.79
GDH-68/13.S-7	540 m	11.76	64.70	05.88	00.00	00.00	00.00	11.76	05.91
GDH-73/19.S-3	437 m	47.05	35.29	05.88	00.00	05.88	00.00	00.00	05.90
GDH-73/19.S-5	441 m	41.17	41.17	11.76	00.00	00.00	00.00	00.00	05.90
GDH-73/19.S-7	454 m	47.05	35.29	05.88	05.90	00.00	00.00	00.00	05.88
GDH-74/19.S-1	435 m	30.00	40.00	10.00	00.00	00.00	00.00	00.00	20.00
GDH-74/19.S-3	458 m	17.64	47.05	05.88	05.88	11.76	00.00	05.88	05.91
GDH-74/19.S-5	481 m	11.76	35.29	05.88	05.88	05.88	05.88	17.64	11.79
GDH-75/20.S-1	427 m	33.33	40.00	00.00	00.00	06.68	00.00	06.66	13.33
GDH-75/20.S-3	437 m	35.29	47.05	05.90	00.00	00.00	00.00	00.00	11.76
GDH-75/20.S-5	444 m	17.64	47.05	05.88	00.00	05.90	00.00	11.77	11.76

Table 4. Chemical properties of iron ore bearing rock, studied area wt.%.

Sample no.	% of Fe_2O_3	Sample no.	% of Fe_2O_3	Sample no.	% of Fe_2O_3	Sample no.	% of Fe_2O_3
GDH-73/19-1	68.07	GDH-73/19-6	77.67	GDH-75/20-1	70.07	GDH-75/20-6	59.25
GDH-73/19-2	63.74	GDH-73/19-7	59.07	GDH-75/20-2	53.74	GDH-75/20-7	66.20
GDH-73/19-3	65.19	GDH-73/19-8	66.98	GDH-75/20-3	75.19	GDH-75/20-8	78.64
GDH-73/19-4	66.99	GDH-73/19-9	63.02	GDH-75/20-4	67.64	GDH-75/20-9	60.20
GDH-73/19-5	59.43	GDH-73/19-10	77.67	GDH-75/20-5	55.00	GDH-75/20-10	46.20

Conclusion

Integrated petrographic, mineralogical, and geochemical investigations of basement cores from four deep drill holes demonstrate the presence of geologically significant iron mineralization within the Precambrian basement of the Masidpur magnetic body, northwestern Bangladesh. Iron-rich horizons occur consistently at depths of approximately 426–548 m and exhibit alternating magnetite- and silica-rich bands with recrystallized metamorphic textures, supporting interpretation of the mineralization as a metamorphosed banded iron formation (BIF). The integrated petrographic, mineralogical, and geochemical evidence indicates that the Masidpur magnetic body shares key characteristics with Precambrian BIF systems recognized worldwide. Comprehensive resource estimation, additional drilling, metallurgical beneficiation testing, and techno-economic and environmental assessments are required to determine its potential economic viability.

Acknowledgement

The authors are grateful to the Director General of the Geological Survey of Bangladesh (GSB) for granting permission to use the laboratory facilities and for providing continuous encouragement and institutional support throughout this study. The authors sincerely thank Zobayer Mahmud, Md. Al Amin, and Md. Abdur Razzaque of GSB for their valuable assistance during the field investigations. They also express their appreciation to the drilling team for successfully collecting the core samples from the Masidpur Magnetic Body. Special thanks are extended to the Economic Geology and Resources Assessment Branch, Geological Survey of Bangladesh (GSB) for its technical and logistical support in the implementation of this research.

References

Ahmed, S.S., Rahman, M.J.J., Uddin, M.K. and Islam, M.S. (2015). Basement tectonics and mineral potential of the Rangpur Saddle, northwestern Bangladesh. *J. Asian Earth Sci.*, **102**: 1-15.

Bish, D.L. and Post, J.E. (1993). Quantitative mineralogical analysis using the Rietveld full-pattern fitting method. *Am. Mineral.*, 78: 932-940.

Boss, C.B. and Fredeen, K.J. (2004). Concepts, Instrumentation and Techniques in Inductively Coupled Plasma Optical Emission Spectrometry. PerkinElmer Life and Analytical Sciences, Shelton, CT.

Chayes, F. (1956). Petrographic Modal Analysis: An Elementary Statistical Appraisal. John Wiley & Sons, New York.

Craig, J.R., Vaughan, D.J., 1994. Ore Microscopy and Ore Petrography, 2nd ed. John Wiley & Sons, New York.

Deer, W.A., Howie, R.A. and Zussman, J. (2013). An Introduction to the Rock-Forming Minerals, 3rd ed. Mineralogical Society, London.

Geological Survey of Bangladesh (GSB) (1990). Geological Map of Bangladesh. Geological Survey of Bangladesh, Dhaka.

Geological Survey of Bangladesh (GSB) (2000). Regional Geophysical (Magnetic) Survey of Northwestern Bangladesh. Unpublished Technical Report. Geological Survey of Bangladesh, Dhaka.

Geological Survey of Bangladesh (GSB) (2012). Detailed Magnetic Survey of the Masidpur–Alihat Area, Hakimpur Upazila, Dinajpur District. Geoscience Project Report. Geological Survey of Bangladesh, Dhaka.

Geological Survey of Bangladesh (GSB) (2013). Geological Drilling Report of Borehole GDH-68/13, Chakupara–Masidpur, Dinajpur District. Geological Survey of Bangladesh, Dhaka.

Geological Survey of Bangladesh (GSB) (2019). Geological Drilling Report of Borehole GDH-73/19, Masidpur Magnetic Body, Dinajpur District. Geological Survey of Bangladesh, Dhaka.

Geological Survey of Bangladesh (GSB) (2020a). Geological Drilling Report of Borehole GDH-74/19, Masidpur Magnetic Body, Dinajpur District. Geological Survey of Bangladesh, Dhaka.

Geological Survey of Bangladesh (GSB) (2020b). Geological Drilling Report of Borehole GDH-75/20, Masidpur Magnetic Body, Dinajpur District. Geological Survey of Bangladesh, Dhaka.

Goldstein, J.I., Newbury, D.E., Michael, J.R., Ritchie, N.W.M., Scott, J.H.J. and Joy, D.C. (2018). Scanning Electron Microscopy and X-ray Microanalysis, 4th ed. Springer, New York.

Goto, A. and Tatsumi, Y. (1994). Quantitative analysis of rock samples by X-ray fluorescence spectrometry (I): Major elements. Journal of the Geological Society of Japan, **100**: 103-115.

Goto, A. and Tatsumi, Y. (1996). Quantitative analysis of rock samples by X-ray fluorescence spectrometry (II): Trace elements. Journal of the Geological Society of Japan, **102**: 795-808.

Gross, G.A. (1980). A classification of iron formations based on depositional environments. Canadian Mineralogist, **18**: 215-222.

Guha, D.K. (1978). Tectonic Framework of Bangladesh. Geological Survey of Bangladesh, Dhaka.

Hutchison, C.S. (1974). Laboratory Handbook of Petrographic Techniques. John Wiley & Sons, New York.

Klein, C. (2005). Some Precambrian banded iron formations (BIFs) from around the world: Their age, geologic setting, mineralogy, metamorphism, geochemistry, and origin. *Am. Mineral.*, **90**: 1473-1499.

Masum M, Hoque M.N, Akbar M.A, Mahmud Z, Rana M.S, Razzaque M.A and Amin M.A. (2021). Geology and Precambrian Banded Iron Formations formed at Rangpur Platform in Bangladesh. *Int. J. Eng. Res. Dev.*, **17**(3): 43-57.

Marjoribanks, R. (2010). Geological Methods in Mineral Exploration and Mining, 2nd ed. Springer, Berlin.

Moon, C.J., Whateley, M.K.G. and Evans, A.M. (2006). Introduction to Mineral Exploration, 2nd ed. Blackwell Publishing, Oxford.

Nesse, W.D. (2017). Introduction to Optical Mineralogy, 5th ed. Oxford University Press, New York.

Potts, P.J. (1987). A Handbook of Silicate Rock Analysis. Blackie, Glasgow.

Rahman M.A, Miah I and H.R. Blank (2000). Digital Processing and Interpretation of Gravity and Magnetic Data, Rangpur-Dinajpur Area, Bangladesh, Record of the Geological Survey of Bangladesh, Vol. 10, Part-1.

Reed, S.J.B. (2005). Electron Microprobe Analysis and Scanning Electron Microscopy in Geology, 2nd ed. Cambridge University Press, Cambridge.

Reimann, K.U. (1993). Geology of Bangladesh. Gebrüder Borntraeger, Berlin.

Rollinson, H.R. (2014). Using Geochemical Data: Evaluation, Presentation, Interpretation, 2nd ed. Routledge, London.

Thompson, M. and Howarth, R.J. (1978). A new approach to the estimation of analytical precision. *J. Geochem. Explor.,* **9**: 23-30.

Young, R.A. (Ed.) (1993). The Rietveld Method. Oxford University Press, Oxford.

Zaher, M.A., Rahman, M.J.J., *et al*., (1980). Verify complete bibliographic information before submission. This reference is cited in the Geological Setting section but is not fully documented in the current manuscript.